Product Catalog	Product Name List	Instrument
Image	Near constant contrast	MERSI-LL
	Nighttime light	MERSI-LL
Cloud and Radiation	Cloud mask	MERSI-LL
	Cloud amount, Cloud type, Cloud phase, Cloud top temperature, Cloud top height/pressure	MERSI-LL
	Outgoing long-wave radiation	MERSI-LL
	Cloud-cleared radiance	HIRAS-II
Atmospheric Sounding	Atmospheric temperature and humidity profiles	MWTS-III, MWHS-II, HIRAS-II
	Dry/wet atmospheric profile	GNOS-II
	Ozone profile	HIRAS-II
	Total precipitable water	MERSI-LL
Atmospheric Dynamic	Ocean vector wind (wind speed/wind direction)	WindRAD
	Sea surface wind speed	GNOS-II
	Polar atmosphere motion vector	MERSI-LL
Land/Sea	Land surface temperature	MERSI-LL
	Sea surface temperature	MERSI-LL
	Snow cover	MERSI-LL
	Sea ice edge & type	WindRAD

***Table 3**. FY-3E Level 2 Science products list. Note that the solar and space weather monitoring products are not included here.*

and nighttime light, sea surface wind field, sea ice edge and type, vertical ozone profile, etc., have been developed.

FY-3E offers certain advantages for the monitoring of trace gases such as CO and O_3 from the hyperspectral infrared observation because of the temperature contrast between the skin temperature and the atmospheric boundary layer that is characteristic of this orbit. The generally smaller amount of cloud and the lower absolute moisture in the early morning can also be an advantage for such air quality monitoring. The early morning orbit also offers the potential to observe the sun in an almost continuous manner. It provides significant advantages for climate monitoring, solar activity, and active regions for space with products such as solar constant, solar spectrum measurements, solar X-ray image, and solar extreme ultraviolet image. Table 3 provides typical Level 2 products from FY-3E. On May 1, 2024, FY-3E was in its operational stage. The data and products can be obtained through the dedicated website, FENGYUN Satellite Data Center (*http://satellite.nsmc.org.cn/portalsite/default.aspx*).

References

Zhang, P., X. Q. Hu, Q. F. Lu, A. J. Zhu, M. Y. Lin, L. Sun, L. Chen, and N. Xu, 2022. FY-3E: The first operational meteorological satellite mission in an early morning orbit. *Adv. Atmos. Sci.*, 39(1), 1–8, *https://doi.org/10.1007/s00376-021-1304-7*.

Zhang, P., X. Hu L. Sun, N. Xu, L. Chen, A. Zhu, M. Lin, Q. Lu, Z. Yang, and J. Wang, 2023. The on-orbit Performance of FY-3E in an Early Morning Orbit. *Bull. Amer. Meteorol. Soc.*, 105(1), DOI: 10.1175/BAMS-D-22-0045.1.

Theoretical Water Balance Research

Allen Hunt
Wright State University, Dayton, OH, USA

Making sense of the patterns of evapotranspiration and associated carbon fluxes across scales and climates forms the basis for the 1st and 2nd goals of Phase 4 of GEWEX, which are to: 1) "Determine the extent to which Earth's water cycle can be predicted," and 2) "Quantify the inter-relationships between Earth's energy, water and carbon cycles." In a series of papers, we develop a firm theoretical foundation for addressing the 1st and 2nd goals, as well as the first step towards addressing the part of the 3rd goal relating to climate change.

Our approach is fundamentally related to network, rather than continuum, representations of soil, for which the fundamental equations are not differential equations, but difference equations. Of course, such a theoretical foundation, which has significant theoretical advantages when compared with the continuum approach to soils, including a greater compatibility with the actual networks that represent plants, has also a significant drawback in its increased difficulty of integration with the usual differential equations that represent the atmosphere and the associated boundary conditions at the Earth's surface.

The highly interdisciplinary research foundation lies in scaling expressions for soil production as a function of time and depth, based on universal understanding of solute transport in porous media as derived in percolation theory, and vegetation growth as a function of time, as related to the optimal paths for root growth through the soil. Both of these scaling functions have been verified by multiple publications in *Ecological Modelling* as well as journals of the following societies: American Chemical Society, American Physical Society, American Geophysical Union, European Geosciences Union, Soil Science Society of America, and the British Society of Geomorphology (e.g., Hunt, 2017; Yu and Hunt, 2017; Egli et al., 2018; Yu et al., 2019; Hunt et al., 2020; Hunt et al., 2021a). The non-linear scaling relationships on which the entire theory is based require incorporation of fundamental length scales (a pore separation, or median particle size, or a plant xylem diameter), and a fundamental time scale. The ratio of the fundamental length scale to the fundamental time scale is the associated hydrologic flux, transpiration (approximated as evapotranspiration, ET) for plant growth, and subsurface run-off, approximated as run-off (streamflow), Q, for soil formation. $Q + ET + \Delta S = P$, with ΔS equal to the annual storage change, then represents the three principal pathways for precipitation, P, on the land surface. Melding the two scaling relationships above provides a basis to develop an expression for the net primary productivity, NPP, which can be used to solve the water balance, generating its direct relevance to the goals of GEWEX.

The work listed above is, despite its relationship with complexity theory, still conventionally described as bottom up, or Newtonian. It is the top-down, or Darwinian component, which then bridges the gap and allows solution of the water balance

equation. In our treatment, the Darwinian perspective is represented by applying ecological optimality. Since the water that continues infiltrating into the soil, passing by the plants, is the foundation for soil formation, and the water that the plants use generates the lateral underground plant growth, one can seek for a principle of ecological optimality to guide the understanding of the partitioning of the water. Plants cannot grow effectively without soil (and the water that infiltrates), but they cannot grow at all without water for transpiration. Nevertheless, these two components of the water balance cannot vary independently, as they must sum to P. The quantitative procedure is to express NPP as the product of two factors, one that is a power of ET (from the fractal dimensionality describing the horizontal architecture of the root mass in a thin soil layer), and one that is a power of (P – ET) for the soil depth, or third dimension. Differentiation of this expression with respect to ET, and setting the result equal to zero, gives the maximum NPP, providing the fraction of P given by ET in the case that neither water limitations, nor energy limitations, exist. This parameter, which relates to the fractal dimensionality of the root system, is the only parameter in the equation. For a 2D root model, this parameter is predicted to be 0.623, and 0.813 for a 3D root model (Hunt et al., 2021b; Hunt et al., 2023a). These two values constrain pretty accurately the observed ET for grasslands and forests around the world (Hunt et al., 2023a).

The above method is adapted to energy-limited systems by applying the optimization only to that fraction of P which could have evaporated (i.e., potential ET, or PET), allowing the remainder of P to run off, while adaptation to systems that are water-limited requires restricting the application of the optimization only to the fraction of ground covered by vegetation, assumed equal to P/PET, and letting the evapotranspiration be 100% over the remaining area. These assumptions represent only the lowest level of assumption, yet the theoretical results produce excellent agreement with data for precipitation elasticity of streamflow (defined below), net primary productivity, and tree species richness (the number of tree species) around the world.

All water balance related comparisons have utilized data at annual timescales or multi-decadal averages. NPP has been compared (Hunt et al., 2024) with data that were originally compiled to represent the latitudinal dependence of NPP in Asia (Budyko, 1974). For precipitation elasticity of streamflow, $\varepsilon_p \equiv (P/Q * dQ/dP)$, Q is generated from actual streamflow, requiring data for Q to come from catchment rather than the climatological data used to determination of aridity index AI ≡ PET/P. Overall, our comparison with four major sources of data covered catchment sizes from 50 km^2 to 7,000,000 km^2, although for the results shown here, the largest catchments were 76,000 km^2. Our predictions for ε_p include the effects of changes in storage, ΔS. We invoked an equal likelihood of positive and negative changes in ΔS to interpret the case ΔS = 0 as being the expected median value of ε_p. For discussion of the ΔS values chosen, see the original paper. For AI < 1, our prediction is that the median ε_p should rise at first slowly, but on the approach to AI = 1, more rapidly, exceeding 2 for a very small range of AI values, then dropping to 2 for AI > 1. This overall dependence is in line with a summary from Chiew (2006).

Climate Zone (Koppen)	Number of Catchments	ϵ_p Median	ϵ_p Range
Tropical (A)	**79**	**1.7**	**(0.8 - 3.1)**
Very wet (Af, Am)	20	1.2	(0.8 - 1.9)
Moderately wet (Aw)	59	2.0	(0.9 - 3.3)
Arid (B)	**45**	**1.8**	**(0.4 - 2.9)**
Cold arid (BWk, BSk)	32	1.6	(0.4 - 3.1)
Warm arid (BWh, BSh)	13	2.0	(0.5 - 2.5)
Temperate (C)	**262**	**1.9**	**(0.9 - 3.1)**
Wet winter (Csa, Csb, Csc)	32	2.0	(0.9 - 3.4)
Wet summer (Cwa, Cwb, Cwc)	35	1.8	(0.8 - 2.8)
No seasonality (Cfa, Cfb, Cfc)	195	1.9	(1.0 - 3.1)
Cold (D)	**135**	**1.1**	**(0.5 - 1.9)**

Table 1*. Statistical characteristics of precipitation elasticity of catchments for various Koppen climate zones.*

For ΔS > 0, however, the prediction for ε_p rises again with increasing AI, generating a second peak in ε_p in the limit of large AI. While evidence of such a double peak is seen clearly in data for ε_p represented as a function of AI (shown by all four major global data sets that could be accessed; Hunt et al., 2023b), the peak at AI = 1 is broadened when ε_p is shown as a function of run-off ratio, Q/P, as in Fig. 1, since AI = 1 corresponds to different Q/P values (horizontal positions) at different values of ΔS. In Fig. 1, this result manifests more as a nonmonotonic curvature in the upper limit of the data. Representing ε_p as a function of Q/P has the advantage of avoiding the necessity of matching distinct data sets. In the figure, the Budyko (1958) function is shown for comparison. While it appears to follow the centroid of the data more closely, its value approaches 4 in the large AI limit (i.e., small Q/P value in Fig. 1), which is not in accord with the tabulated data. Our predictions for each value of ΔS are cut off at the maximum AI value reported in the data set and do an excellent job of reproducing the entire field occupied by the

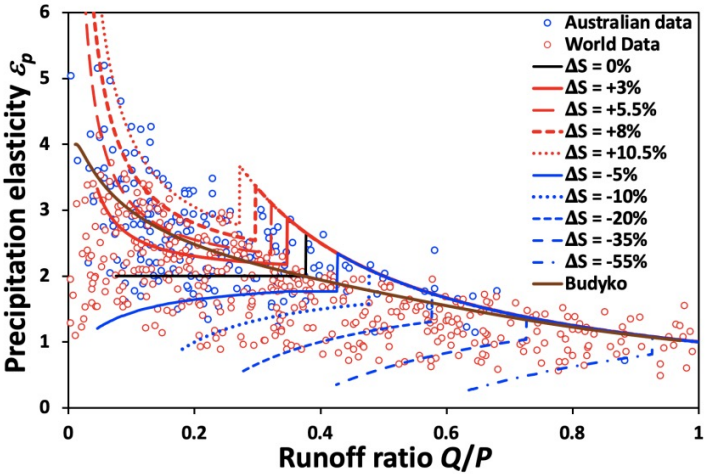

Figure 1*. Comparison of precipitation elasticity* $\varepsilon_p \equiv (P/Q * dQ/dP)$ *developed from the analytical solution of the water balance, including annual storages (of the percentages listed) with data for the dependence of elasticity on runoff coefficient from the publications of Chiew (Hunt et al., 2023b). Note that* ΔS = 0 *is expected to generate a median value of* ε_p*, which is confirmed by comparison with tabulated values across climate regimes in Hunt et al. (2023b).*

data. Clearly, for a meaningful prediction of precipitation elasticity of streamflow and, by inference, the water balance itself, changes in shallow subsurface storage must be accounted for.

Comparisons across such a wide range of scales also revealed an important and physically sensible result, that the storage change values necessary to constrain the observations decreased with basin area to values less than 10% at the largest scales.

I would like to conclude with a quote from the *Eos* highlight (*https://eos.org/editor-highlights/how-much-terrestrial-precipitation-is-used-by-vegetation*) of Hunt et al. (2023b): "The contribution allows us to predict the impact of changing climatic conditions on the interplay between climate, vegetation, and water resources. The findings open the door to new perspectives in climate change impact assessment."

References

Budyko, M.I., 1958. *The heat balance of the Earth's surface*. Translated by N.A. Stepanova. U.S. Department of Commerce, Weather Bureau.

Budyko, M.I., 1974. *Climate and life*. International Geophysics Series 18. Academic Press, New York.

Chiew, F.H.S., M.C. Peel, T.A. McMahon, and L.W. Siriwardena, 2006. Precipitation elasticity of streamflow in catchments across the world. In (S. Demuth, A. Gustard, E. Planos, F. Scatena, and E. Servat,eds.) *Climate Variability and Change: Hydrological Impacts* (pp. 256–262), International Association of Hydrological Sciences.

Egli, M., A.G. Hunt, D. Dahms, G. Raab, C. Derungs, S. Raimondi, and F. Yu, 2018. Prediction of soil formation as a function of age using the percolation theory approach. *Front. environ. sci.*, 28. *https://doi.org/10.3389/fenvs.2018.00108*.

Hunt, A.G., 2017. Spatio-temporal scaling of vegetation growth and soil formation: Explicit predictions. *Vadose Zone J*. DOI:10.2136/vzj2016.06.0055

Hunt, A.G., B.A. Faybishenko, and T.L. Powell, 2020. A new phenomenological model to describe root-soil interactions based on percolation theory. *Ecol. Model.* 433: 109205.

Hunt, A.G., B.A. Faybishenko, and B. Ghanbarian, 2021a. Non-linear hydrologic organization. *Nonlin. Processes Geophys.*, 28, 599–614. *https://doi.org/10.5194/npg-28-599-2021*.

Hunt, A.G., B. Faybishenko, and B. Ghanbarian, 2021b. Predicting characteristics of the water cycle from scaling relationships. *Water Resour. Res.* 57: e2021WR030808.

Hunt, A.G., M. Sahimi, B.A. Faybishenko, M. Egli, B. Ghanbarian, and F. Yu, 2023a. Interpreting water demands of forests and grasslands within a new Budyko formulation of evapotranspiration using percolation theory. *Sci. Total Environ.*, 877, 162905.

Hunt, A.G., M. Sahimi, and B. Ghanbarian, 2023b. Predicting streamflow elasticity based on percolation theory and an ecological optimum. *AGU Adv.*, in press.

Hunt, A.G., M. Sahimi, and B. Ghanbarian, 2024. Predicting ecosystem net primary productivity by percolation theory and optimality principle. *Water Resour. Res.*, 60(3). DOI: 10.1029/2023WR036340.

Yu, F., and A.G. Hunt, 2017. An examination of the steady-state assumption in certain soil production models with application to landscape evolution. *Earth Surf. Process. Landf.* DOI: 10.1002/esp.4209.

Yu, F., A.G. Hunt, M. Egli, and G. Raab, 2019. Comparison and contrast in soil depth evolution for steady-state and stochastic erosion processes: Possible implications for landslide prediction. *Geochem. Geophys. Geosyst*. *https://doi.org/10.1029/2018GC008125*.

Asian Summer Monsoon Variability during 2022–2023: Beyond Canonical Teleconnection Patterns

R.S. Ajayamohan[1], Gill Martin[2], Thea Turkington[3], Hatsuki Fujinami[4], Joseph Basconcillo[5], H. Annamalai[6], Shiromani Jayawardena[7], Raghavendra Ashrit[8], Hiroshi Takahashi[9], and Tieh Yong Koh[10], on behalf of the CLIVAR/GEWEX Regional Working Group on Asian-Australian Monsoons

[1]NYU Abu Dhabi, UAE; [2]Met Office, UK; [3]CCRS, Singapore; [4]ISEE, Nagoya University, Japan; [5]PAGASA, Philippines; [6]IPRC, University of Hawaii, USA; [7]Climate Change Secretariat, Sri Lanka; [8]NCMRWF, India; [9]Tokyo Metropolitan University, Japan; [10]Department of Applied Mathematics and Theoretical Physics, University of Cambridge, UK

The boreal summer monsoon, a seasonal phenomenon vital to the world's most populous regions, paints a broadly contrasting picture between the years 2022 and 2023 (Figs. 1a-b). For example, climatologically dry regions of Pakistan and surrounding Gulf countries received unprecedented rainfall during 2022, resulting in devastating floods, while in 2023, much of the region saw drier conditions overall but did not exhibit the typical El Niño teleconnection pattern. Here, members of the Climate and Ocean-Variability, Predictability, and Change (CLIVAR)/GEWEX Monsoons Panel and Regional Working Group on Asian-Australian Monsoons (WG-AAM) highlight the need for better understanding and predicting monsoon variability at regional scales in a warming planet.

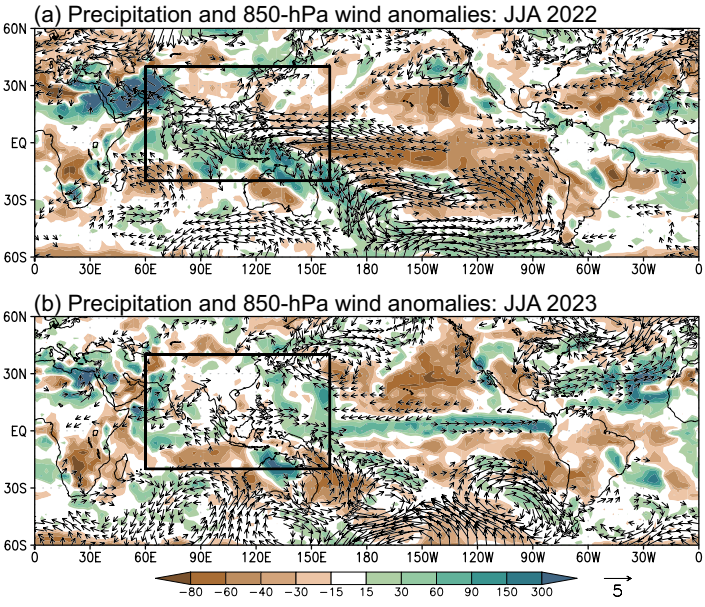

***Figure 1**. (a) Anomalies in precipitation (% difference against climatology) and 850hPa wind fields (vectors; m s^{-1}) in 2022 summer (June–August). Wind anomalies less than 1.0 m s^{-1} are omitted. (b) As in (a) but for 2023. Anomalies are estimated with respect to the climatological mean (1991–2020). The black box (60–160°E, 20°S–40°N) indicates Asian-Australian monsoon region. Precipitation: Global Precipitation Climatology Project (GPCP) Version 2.3. Wind fields: Japanese Reanalysis for Three-Quarters of a Century (JRA 3Q)*